frontiers | Frontiers in Earth Science

TYPE Original Research
PUBLISHED 30 May 2023
DOI 10.3389/feart.2023.1093020

OPEN ACCESS

EDITED BY
Babalola Ogunsua,
Chinese Academy of Sciences (CAS), China

REVIEWED BY
Abhay Srivastava,
North Eastern Space Application Centre, India
Oladipo Abe,
Federal University Oye-Ekiti, Nigeria
Louis Osei-Poku,
Hong Kong Polytechnic University Kowloon, China in collaboration with reviewer OA

*CORRESPONDENCE
Qilin Zhang,
qlzhang@nuist.edu.cn
Jinquan Zeng,
58803572@qq.com

RECEIVED 08 November 2022
ACCEPTED 04 May 2023
PUBLISHED 30 May 2023

CITATION
Zhou J, Zhang Q, Song L, Zhang J, Dai B, Li J, Yang J, Wang Y, Gu J and Zeng J (2023), On the improvement of the single-site lightning distance estimation by using the time-delay correction. *Front. Earth Sci.* 11:1093020. doi: 10.3389/feart.2023.1093020

On the improvement of the single-site lightning distance estimation by using the time-delay correction

Jiahao Zhou[1], Qilin Zhang[1]*, Lin Song[2], Junchao Zhang[1], Bingzhe Dai[1], Jie Li[1], Jing Yang[1], Yao Wang[1], Jiaying Gu[1] and Jinquan Zeng[3]*

[1]Collaborative Innovation Center on Forecast and Evaluation of Meteorological Disasters (CIC-FEMD)/Jiangsu Collaborative Innovation Center of Atmospheric Environment and Equipment Technology (CICAEET)/Key Laboratory for Aerosol Cloud-Precipitation of China Meteorological Administration, Nanjing University of Information Science and Technology, Nanjing, China, [2]Qingdao Ecological and Agricultural Meteorological Center, Qingdao, China, [3]Fujian Meteorological Disaster Defense Technology Center, Fuzhou, China

Due to the propagation effect, the arrival time of the ground wave peak is delayed when sferics propagate at long distances. In this work, we propose a new method combined with a numerical algorithm to correct the effect of the ground wave peak time delay and calculate the ionosphere height using the difference between the arrival time of the ground wave and the skywave. The results showed that, with each increase of the propagation distance by 100 km, the delay in arrival time of the ground wave peak increased by an average of 0.9 μs. For the first and second reflectance heights, the maximum heights observed at night were 86 km and 89 km, and the minimum heights during the day were 66 km and 69 km, respectively. Using the difference in arrival time between the ground wave and skywave and the ionosphere equivalent reflection height, a single site was used to estimate the distance of lightning occurring within 900 km. This method had an average relative error of 14.6%, an average absolute error of 128.8 km, and a median distance error of 52.6 km. Finally, the percentage of data with an estimated deviation within 10% increased from 52% to 65%.

KEYWORDS

ground wave peak time delay, ionospheric reflection height, single-site, lightning distance estimation, lightning location

1 Introduction

The ionosphere D region is usually considered to be the atmospheric plasma layer at an altitude of 50–90 km above the ground, which is ionized by solar radiation and contains free electrons (Cummer et al., 1998). Due to the presence of electrons and ions, the ionosphere can reflect extremely-low-frequency (ELF; 3–3000 Hz) and very-low-frequency (VLF; 3–30 kHz) electromagnetic waves, which are commonly known as sferics (a shortened form of atmospherics). Sferics travel thousands of kilometers in the Earth–ionosphere waveguide (EIWG) with little attenuation (~2–3 dB/1,000 km) (Ammar and Ghalila, 2020). Therefore, sferics have been widely used to examine ionosphere reflection characteristics (Inan et al., 2010). Since the development of

detection technology in recent years, studying the ionosphere D region using sferics has also become a vital detection technology.

Smith et al. (2004) used VLF/LF electric-field-change signals recorded by the Los Alamos Sferic Array (LASA) to calculate the height of the ionosphere. On this basis, Jacobson et al. (2008) analyzed the effects of solar zenith angle, electromagnetic wave propagation distance, and propagation orientation on the ionosphere height. Lay and Shao (2011a), Lay and Shao (2011b), and Shao et al. (2013) used multi-station lightning location results to invert the temporal and spatial variations of ionosphere heights in the region near a large thunderstorm. The results showed that the height of the inverse ionosphere reflection exhibited temporal and spatial fluctuations even in the absence of thunderstorms beneath these regions. The phase propagation velocity of these fluctuations ranged from 45 to 85 m/s. It lasted for several hours, suggesting that it may be due to the perturbation of the ionosphere by the gravity waves of the thunderstorm. Tran et al. (2017) computed the vertical electric field and azimuthal magnetic field at distances of 50 to 500 km from the lightning channel using the 2-D FDTD method and estimated the apparent ionosphere reflection heights. The model predicted that within 300 km in the nighttime and 200 km in the daytime, the apparent reflection heights are within approximately 10% of the reference height h0 for both the first and the second skywaves. Azadifar et al. (2017) calculated the ionosphere reflection height using the waveform of the electric field generated by the upward lightning flash at a distance of 380 km. The difference between the arrival times of the ground wave and skywave was used to estimate ionosphere reflection height during day and night times, based on the so-called peak-to-peak and zero-to-zero methods. Zhou et al. (2021) assumed a parameter T_0 as the ground wave time delay, with values ranging from 0 to 25 μs and a step of 0.1 μs to meet the accuracy requirement. However, the exact relationship between the time delay and the propagation distance was not precisely determined. To improve lightning location accuracy, the ground-based lightning location network (LLN) uses multiple electromagnetic pulse detection sites. However, in some exceptional cases, for example, in the absence of a highly precise timing system or when the data cannot be transferred to the server, a single site can be used to determine the location of the lightning; this method can also help save operation and maintenance (O&M) costs (Wang et al., 2022). An important issue that deserves attention is how to improve the accuracy and efficiency of the single-site lightning location. Ramachandran et al. (2007) described a method based on lightning-generated VLF sferics received in a single site, with an average error in distance estimation of 8.8%. Ogawa and Komatsu (2007) discovered that it is possible to observe a secondary waveform caused by the same lightning strikes by examining the background noise from 1 Hz to 11 kHz. The secondary (antipodal) waveform is the consequence of the sferics traveling around the world in the other direction. Using both direct and secondary waveforms, lightning location can be determined although secondary waveforms are often difficult to identify. To overcome these problems, Koochak and Fraser Smith (2020) introduced a lightning location method that worked by processing the sferics to determine the arrival times of the VLF and ELF radiation components. Using these two individual arrival times, we can approximate the distance that the sferics propagate in the EIWG. Mostajabi et al. (2019) proposed a novel source localization technique based on electromagnetic time reversal (EMTR) and machine learning (ML). With the novel method, precise 2D lightning location is possible with just one sensor; however, it is limited by the necessity of the presence of scatterers.

The time difference between the ground wave and the skywaves can be used to calculate the reflection height of the ionosphere D region and estimate the distance of lightning. However, due to the curvature of the Earth and the finite conductivity of the ground, when the electromagnetic waves generated by lightning propagate along the ground, the ground wave will be attenuated. As propagation distance increases, the arrival time of the ground wave significantly lags the arrival time of the speed of light; thus, the actual time difference between the ground wave and the skywaves should be larger than that in the waveform data. Therefore, this work proposes a new method combined with a numerical algorithm to correct the ground wave time delay due to long-distance propagation to calculate a more reliable reflection height of the ionosphere D region. Moreover, the ionosphere reflection height combined with the arrival time difference between the ground wave and the skywaves can estimate the distance of the lightning source from a single site.

2 Data analysis method

2.1 Description of the experimental instrument and data

Based on a long-range lightning location network with a very-low-frequency band that we have established in China (Li et al., 2022), the original magnetic field waveform data are recorded and sent to the server as long as it exceeds the minimum threshold with a sampling rate of 1 MS/s. The modified empirical wavelet transform (MEWT) method based on the empirical wavelet transform (EWT) is used for the azimuthal magnetic fields field signal de-noising. A GPS receiver at the station provided a one-pulse-per-second (1 PPS) output as a reference source for tagging data sample times, with an accuracy of ±50 ns. Our previous work compared our lightning location results with the advanced direction-time lightning detection (ADTD) system. Compared with ADTD, the average location error was 4.32 km, with a standard deviation of 2.46 km (Zhang et al., 2022).

Since various time zones affect the sunlit point, the electron concentration in the ionosphere will vary depending on the location, which could result in variations in the ionosphere's equivalent reflection height. To obtain the complete curve of the ionosphere reflection height with time, we chose data within a region, as shown in Figure 1A, in which 6612 lightning strikes were recorded 430 km–1,240 km from the Nanjing station. The characteristics of the first and second skywaves in the sferics can be more clearly distinguished within this range, and we distinguished the time stamps of lightning by colors. Additionally, as shown in Figures 1B–D, we chose data from

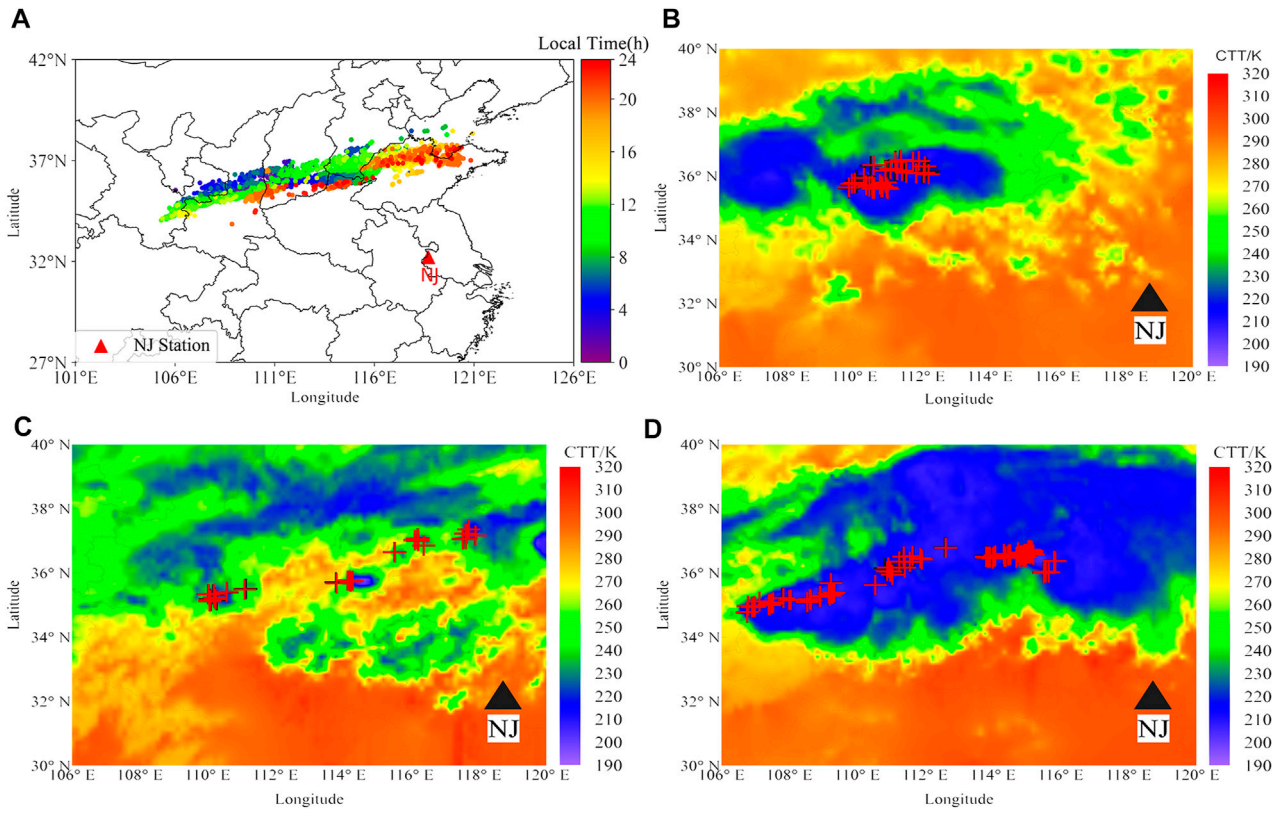

FIGURE 1
istribution of lightning events in selected regions on 3 October 2021(local time: UT+8) **(A)** from 00:00 to 23:59; **(B)** from 02:00 to 02:15; **(C)** from 09:00 to 09:15; and **(D)** from 20:00 to 20:15.

three distinct times and contrasted them with cloud top temperature (CTT) data obtained by the Advanced Geosynchronous Radiation Imager (AGRI) carried by Feng Yun IV. The black cross in the figure represents our multi-station lightning location results, while the red cross represents ADTD's lightning location results. The dark blue area in the figure indicates a lower CTT value of the area and NJ is the single site we built. The lightning events were all observed in the cloud regions with CTT at about 210–220 K, suggesting a reasonable location accuracy. The good overlay of data from different periods with CTT and ADTD lightning location results further illustrates the reliability of the data.

2.2 Ground wave peak delay *versus* distance

The arrival time and waveform of the electromagnetic waves are different from those under ideal ground conditions when the low-frequency (LF)/VLF electromagnetic waves radiated by the lightning discharge travel along the Earth's surface because the electromagnetic waves propagated over long distances are affected by the irregular ground conductivity distribution on the propagation path, complex terrain, and other factors. Numerous observations and simulations support this phenomenon (Shao and Jacobson, 2009; Hou et al., 2020). The error in calculating the ionosphere reflection height and estimating the lightning distance by a single site using the time differential between the ground wave and the skywave will rise as the propagation distance increases. The ground wave arrival time delay caused by an increase in propagation distance is referred to in this study as t_d.

The background noise that interferes with the sferics during propagation comes from a variety of sources, including the power supply, the thermal noise of the device, the interference noise between the lines, the external noise brought by the signal transmitter around the station, the high-voltage power supply line, and equipment that does not consider electromagnetic compatibility, which makes it more difficult to identify the peak of the ground wave and the skywaves. A two-dimensional finite difference time domain (FDTD) model was used to simulate the propagation of sferics in EIWG to precisely determine the peak sites of the ground wave and the skywaves of the actual sferics waves. This simulation was conducted under typical daytime and nighttime ionosphere conditions at propagation paths of 100 km–3,000 km. The size of the FDTD simulation domain was 3,200 km × 100 km, the space step was set to $\Delta r = \Delta z = 500$ m, the time step Δt was 1 μs to ensure the same time resolution as the observed data, and the length of the lightning channel was 10 km. The reference height of the ionosphere was set to 70 km for the daytime condition and 85 km for the nighttime condition. The density of positive ions was set to the same value as the electrons but with a minimum value of 200 cm^{-3} for the daytime condition and 100 cm^{-3} for the nighttime condition. The parameter settings of the simulations

matched those of Li et al. (2022), Hou et al. (2018), and Hou et al. (2020). We used this model to simulate the propagation of VLF lightning electromagnetic waves in EIWG and establish a waveform bank containing simulated lightning waveforms with different propagation distances (from 100 km to 3,000 km, with a distance interval of 100 km).

It is simple to identify the peak points of the ground wave and skywaves on the simulated waveforms because they were created under perfect conditions. Following that, using the method suggested by Carvalho et al. (2017), the peak points of the ground wave and skywaves in the simulated waveform bank were determined by identifying the fast and slow breakpoints in the waveform. The waveform in the simulated waveform bank with the highest correlation coefficient to the real sferics waveform was found using the cross-correlation technique. The peak points of the simulated waveform were determined to accurately identify the peak points of the ground wave and skywaves of the actual waveform; we set the length of the sliding time window to 10 μs, centering on the peak points of the simulated waveform and searched for the peak points of the actual sferics waveform within the time window. This method was also used by Li et al. (2022), in which the peak point of the ground wave was obtained by matching. The matching approach can still precisely identify the peak spots of the ground wave and skywaves even though the sferics is impacted by noise, and there are some differences between the actual and matched waveforms in the waveform bank. The peak points of some actual waveforms, however, might appear not within the time window due to noise interference; this part of the data was not used in the following work in the present study.

2.3 Time delay revision

We used a model simulation based on the theories of ground wave propagation along the spherical Earth surface with finite conductivity proposed by Hill and Wait to account for the propagation (Hill and Wait, 1980).

When both finite ground conductivity and the curved surface of the Earth are considered, the attenuation factor in the frequency domain is calculated as (Wait, 1974)

$$W = e^{-j\pi/4}\sqrt{\pi x}\sum_{s=1}^{\infty}\frac{e^{-jxt_s}}{t_s - q^2}, \tag{1}$$

$$x = (k_0R/2)^{\frac{1}{3}}(d/R), \tag{2}$$

$$q = -j(k_0R/2)^{\frac{1}{3}}\Delta, \tag{3}$$

$$\Delta = k_0/k\sqrt{1-(k_0/k)^2}, \tag{4}$$

$$k = \omega\sqrt{\varepsilon_r\varepsilon_0\mu_0 - j\sigma\mu_0/\omega}, \tag{5}$$

In Eqs 1–5: t is the normalized ground surface impedance, k is the wave number of electromagnetic waves in the soil, k_0 is the wave number of electromagnetic waves in the vacuum, d is propagation distance, R is the radius of the Earth, ω is the angular frequency, ε_0 and μ_0 are the dielectric constant and magnetic permeability in the air, respectively, ε_r and σ are the relative dielectric constant and conductivity of the ground, respectively, and t_s is the roots of the complex equation. The complex equation is

TABLE 1 Typical lightning current waveform parameters of the first and subsequent RS.

Type	First RS	Subsequent RS
i_{01} (kA)	28	10.7
τ_{11} (μs)	1.8	0.25
τ_{12} (μs)	95	2.5
i_{02} (kA)	-	6.5
τ_{21} (μs)	-	2
τ_{22} (μs)	-	230

$$w_1'(t) - qw_1(t) = 0. \tag{6}$$

$w_1(t)$ is expressed as

$$w_1(t) = \sqrt{\pi}\left(Bi(t) - jAi(t)\right), \tag{7}$$

where $Ai(t)$ and $Bi(t)$ are the Airy functions.

This study considered three current waveforms, corresponding to typical first return stroke (RS), subsequent RS, and dipole source waveforms. We calculated the spatial-temporal distribution of the lightning current along the channel by using the modified transmission line model with exponential current decay with height (MTLE) mode (Nucci et al., 1988). The current source waveforms for the first and subsequent RS were in the form of a double Heidler function (Heidler et al., 1999), assuming that the amplitude decreased exponentially with increasing height as the lightning current travels up the lightning channel, while the return stroke current waveform of dipole source was assumed to be uniform along the lightning discharge channel (Hu and Cummer, 2006). The lightning channel length H was set to 7.5 km and the ground conductivity σ was assigned a typical value of 0.01 S/m.

Table 1 shows the typical lightning-based current waveforms of the first and subsequent RS commonly used in engineering calculations (Rachidi et al., 2001).

i_{01} and i_{02} are the peak currents of the breakdown current and corona current, respectively, τ_{11} and τ_{12} are the rising and falling edge times of the breakdown current, respectively, and τ_{21} and τ_{22} are the rising and falling edge times of the corona current, respectively.

The RS current waveform of the dipole source was assumed to be uniform along the lightning discharge channel as follows:

$$I(t) = I_0\frac{v_0}{\gamma}\left[e^{-at} - e^{-bt}\right]\left[1 - e^{-\gamma t}\right]\Big/H, \tag{8}$$

where $I_0 = 20$ kA, $v_0 = 8 \times 10^7$ m/s, $\gamma = 3 \times 10^4 s^{-1}$, $a = 2 \times 10^4 s^{-1}$, $b = 2 \times 10^5 s^{-1}$, and H is the lightning discharge channel length (Dennis and Pierce, 1964; Hu and Cummer, 2006).

Figure 2A shows the current waveforms of the typical first and subsequent RS. Compared with the first RS, the rising edge of the subsequent RS is steeper and contains more high-frequency components. Figure 2B shows the current waveforms of the dipole source.

Figures 2C–E show simulated waveforms at different distances and the time difference between the peak time of the ground wave and d/c (d is the propagation distance and c is the

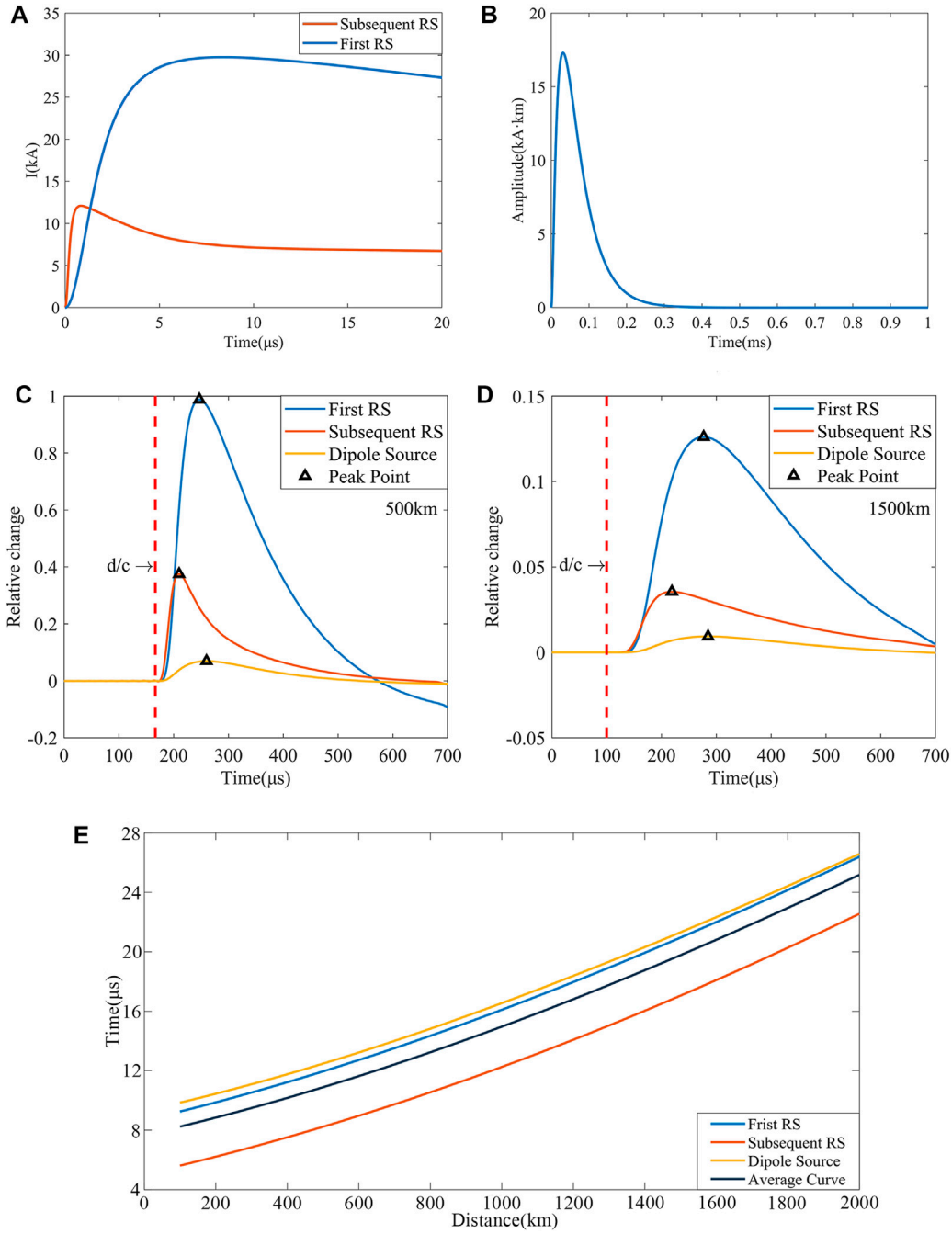

FIGURE 2
ightning current waveforms and time delay *versus* distance curves. **(A)** Current waveforms of the typical first RS and subsequent RS. **(B)** The current waveform of the dipole source. **(C)** Simulated waveforms of different current sources at 500 km. **(D)** Simulated waveforms of different current sources at 1500 km. **(E)** Delay in ground wave peak arrival time compared to *d*/*c*.

speed of light) for the different lightning current sources, which is the difference between the ideal and actual ground wave arrival times. This time difference is also known as t_d, as defined previously. The simulated waveforms at 500 km and 1,500 km, respectively, are shown in Figures 2C, D. A black triangle indicates the ground wave peak point for each current source, while the vertical red dashed line represents the ground wave arrival time in the ideal case (*d*/*c*). The time difference between the peak point and *d*/*c* grows as the distance increases, and the ground wave arrival time of the subsequent RS is always earlier than the other two current sources. Figure 2E shows that the delay time grows almost linearly with distance and that there is no significant difference between the three current sources. The subsequent RS contains more high-frequency components compared to the other two current sources, the rising edge of the current source waveform of the subsequent RS is more jittery,

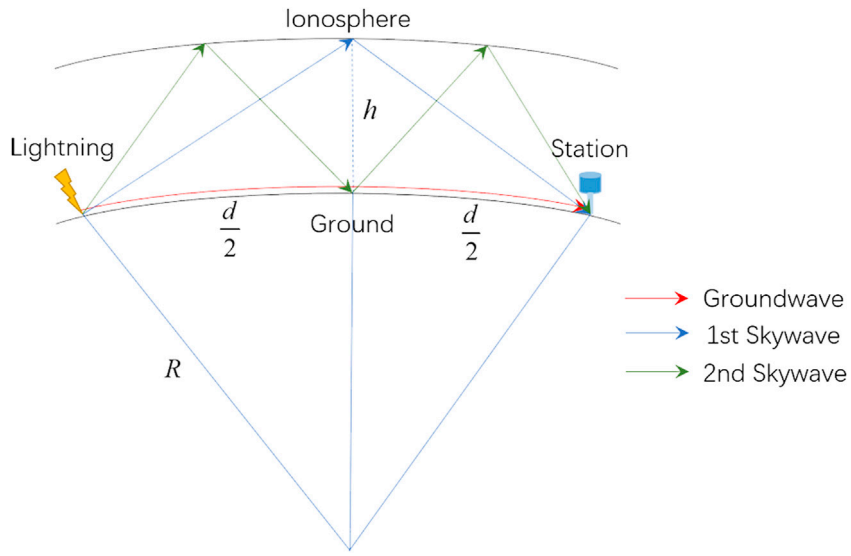

FIGURE 3
Schematic diagram of the first and second skywave reflections in EIWG.

and the peak point arrives earlier than the other two current sources. Because the frequency bands of the three current sources differ, the high-frequency components will arrive earlier than the low-frequency components during propagation. Further statistical results showed that the peak arrival time was delayed by an average of 0.9 μs for every 100 km increase in propagation distance of the lightning electromagnetic waves. The ground wave arrival time delay cannot be ignored when determining the ionosphere reflection height using long-distance lightning.

2.4 Inverse ionosphere reflection height

The geometric model of sferics propagation in the EIWG is given in Figure 3. The sferics propagate in the EIWG through multiple specular reflections from the Earth's surface and the ionosphere D layer. The sferics propagating along the ground is the ground wave, while the sferics reflected by the ionosphere is the skywave. The model assumes that the ground is a good conductor and that electromagnetic waves propagate at the speed of light. The ionosphere equivalent reflection height can be determined (Wait, 1974) by considering the geometric relationship between the ground wave and skywave and the difference in their arrival times.

The reflection height of the first skywave (H_1) can be derived as follows (Somu et al., 2015):

$$H_1 = R\left[\cos\left(\frac{d}{2R}\right) - 1\right] + \sqrt{\left\{R^2\left[\cos^2\left(\frac{d}{2R}\right) - 1\right] + \left(\frac{ct_1 + d}{2}\right)^2\right\}}. \tag{9}$$

Similarly, the expression of the second skywave reflection height (H_2) can be derived as follows:

$$H_2 = R\left[\cos\left(\frac{d}{4R}\right) - 1\right] + \sqrt{\left\{R^2\left[\cos^2\left(\frac{d}{4R}\right) - 1\right] + \left(\frac{ct_2 + d}{4}\right)^2\right\}}. \tag{10}$$

In Eqs 9, 10, R is the radius of the Earth, d is the spherical distance between the lightning and the station, c is the speed of light in free space, t_1 is the arrival time difference between the ground wave and the first skywave, and t_2 is the arrival time difference between the ground wave and the second skywave.

However, when the lightning propagates long distances, using the aforementioned equation, a certain error is present due to the ground wave peak time delay. Previous research demonstrated that propagation over the land for a distance of about 130 km with a conductivity of 3 mS/m resulted in an average peak of RS pulse delay of 1.8 μs (Honma et al., 1998). According to the simulation results of Shao and Jacobson (2009), the leading edge and the peak were delayed by 5 μs and 13 μs, respectively, at a distance of 1,000 km. In general, electromagnetic wave propagation over terrain with lower ground conductivity results in a larger arrival time delay. The present study considered a ground wave arrival time delay caused by the propagation effect, with the theoretical time difference between the arrival time of the skywave and the ground wave assumed to be T. The time difference between the skywave and the theoretical ground wave should be expressed as (Eqs 11, 12)

$$T_1 = t_1 + t_d, \tag{11}$$

$$T_2 = t_2 + t_d, \tag{12}$$

where t_d is the ground wave peak time delay in a certain distance obtained from Figure 2E; and t_1 and t_2 are the time differences between the actual ground wave and the first and second skywaves, respectively, which is the time difference between the skywaves and the ground wave in the received waveform. The equation for determining the ionosphere equivalent reflection height after the

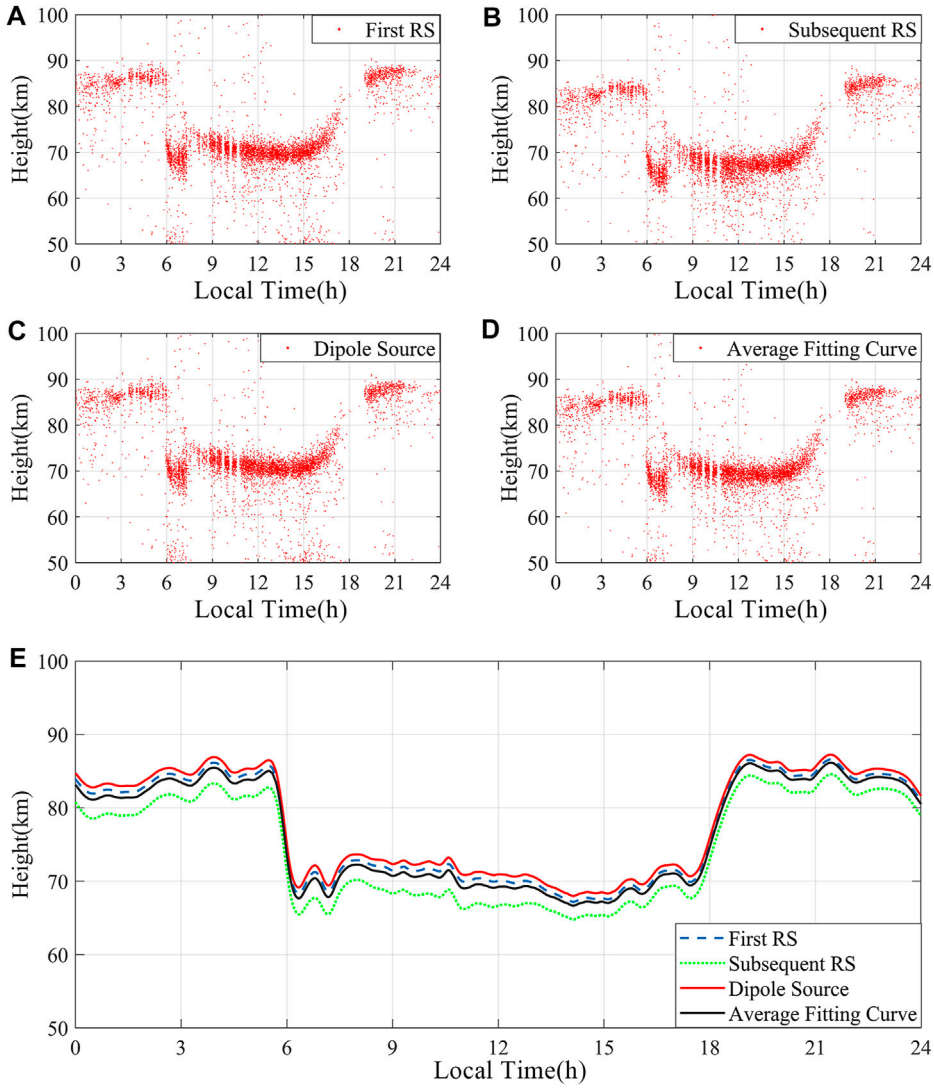

FIGURE 4
Scatter plot and a line graph of H_1 plotted by revising the ground wave arrival time using the time delay curves obtained from different current sources (local time: UT+8). **(A)** First RS. **(B)** Subsequent RS. **(C)** Dipole source. **(D)** Average fitting curve. **(E)** Line graph of H_1 plotted by four revised curves.

ground wave arrival time delay has been revised and can be calculated by substituting Eqs 11, 12 into Eqs 9, 10:

$$H_1 = R\left[\cos\left(\frac{d}{2R}\right) - 1\right] + \sqrt{\left\{R^2\left[\cos^2\left(\frac{d}{2R}\right) - 1\right] + \left(\frac{cT_1 + d}{2}\right)^2\right\}}, \quad (13)$$

$$H_2 = R\left[\cos\left(\frac{d}{4R}\right) - 1\right] + \sqrt{\left\{R^2\left[\cos^2\left(\frac{d}{4R}\right) - 1\right] + \left(\frac{cT_2 + d}{4}\right)^2\right\}}. \quad (14)$$

We substituted the distance (d) and the revised time difference between the skywave and ground wave (T_1, T_2) of the lightning event occurring into Eqs 13, 14 to calculate the continuous 24-h variation of the ionosphere equivalent reflection height and estimated the distance between the lightning strike point and a single site.

To determine the continuous 24-h variation of the ionosphere equivalent reflection height and calculate the distance between the lightning strike point and single site, we substituted the distance (d) and the revised time difference between the skywave and ground wave (T_1, T_2) of the lightning event occurring in Eqs 13, 14.

We applied the results discussed previously to the lightning events that occurred between 00:00 and 23:59 on 13 October 2021, to invert the day-by-day variation of the ionosphere equivalent reflection height. The distances of the lightning data used in this paper from Nanjing station ranged from 430 km to 1240 km. The altitudes of the source and receiving stations were neglected in the computation. The precision of the computation results was unaffected by treating the height as 0 km.

Figures 4, 5 show the ionosphere equivalent reflection height (H_1, H_2) using the time difference between the first skywave, the second skywave, and the revised ground wave, respectively. Figures 4A–C are scatter plots of H_1 inversion after revising

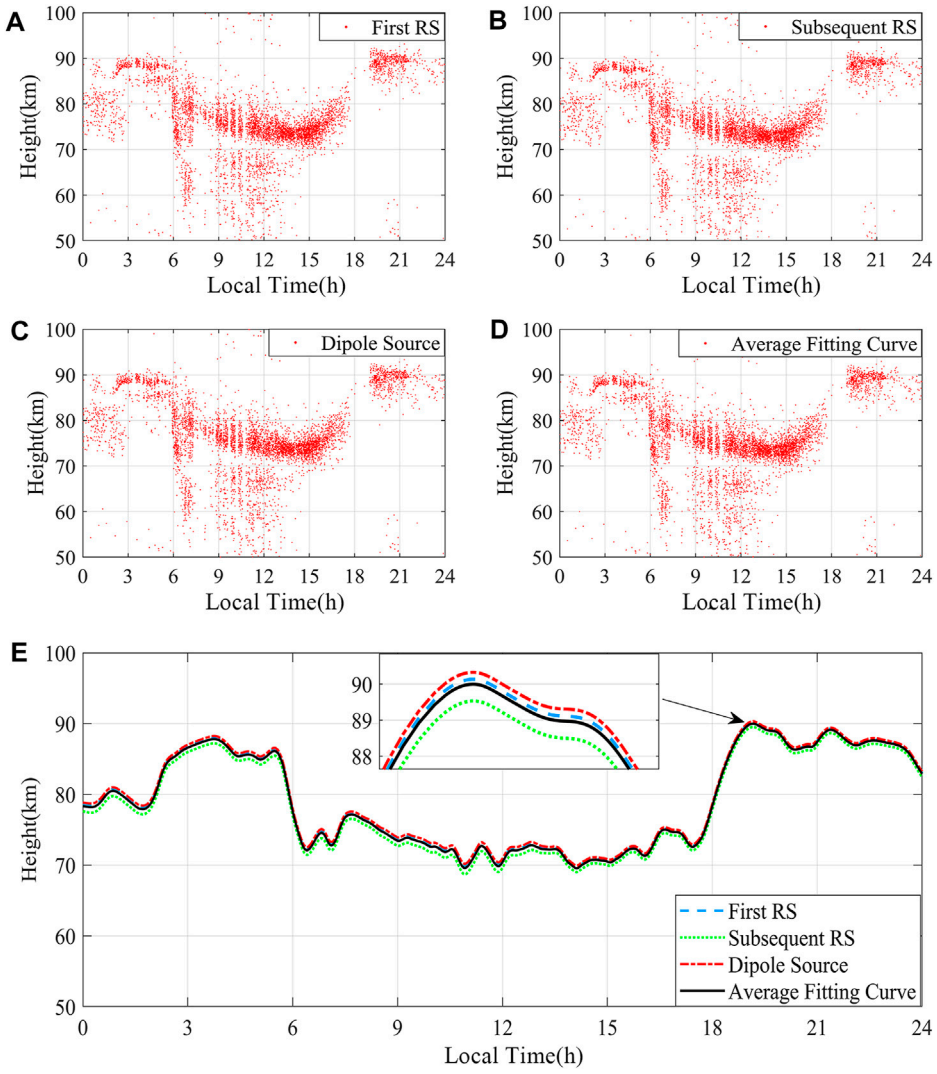

FIGURE 5
Scatter plot and a line graph of H_2 plotted by revising the ground wave arrival time using the time delay curves obtained from different current sources (local time: UT+8). **(A)** First RS. **(B)** Subsequent RS. **(C)** Dipole source. **(D)** Average fitting curve. **(E)** Line graph of H_2 plotted by four revised curves.

the ground wave arrival time using the time delay curves obtained from different current sources. Figure 4D shows the average fitting results for the three current sources. Figure 4E is a line graph fitted from the aforementioned scatter plots, in which the results of the first RS and the dipole source (blue and red curves) are close, except for the relatively low subsequent RS (green curve). The average fitted curve (black curve) is in the middle of the other three curves.

Figures 5A–C are scatter plots of H_2 obtained by fitting the time delay curves using different current sources, respectively. Figure 5D shows the average fitting results for the three current sources. Figure 5E is a line graph fitted from the aforementioned scatter plots. After using the time delay curves to revise the ground wave arrival time, the H_2 obtained using the time difference between the second skywave and ground wave is very close and almost overlaps in Figure 5E.

Figure 2 shows that the t_d obtained by the subsequent RS is smaller than other current sources; therefore, the ionosphere equivalent reflection height calculated using the time difference between ground waves and skywaves is also lower, as reflected in Figures 4, 5. At the same time, the height gap of the H_2 curve calculated after the revision of t_d obtained by different current sources was much smaller than that of H_1 because in the range of 430 km–1240 km, the time difference between the second skywave and the ground wave (T_2) was much larger than the time difference between the first skywave and the ground wave (T_1), and t_d had less influence on T_2. Since the effect of revision in T_2 was not very apparent, we chose the time difference between the first skywave and the ground wave when estimating the lightning distance for a single site.

In both the time delay *versus* distance curves (Figure 2) and the ionosphere equivalent reflection heights (Figures 4, 5), the

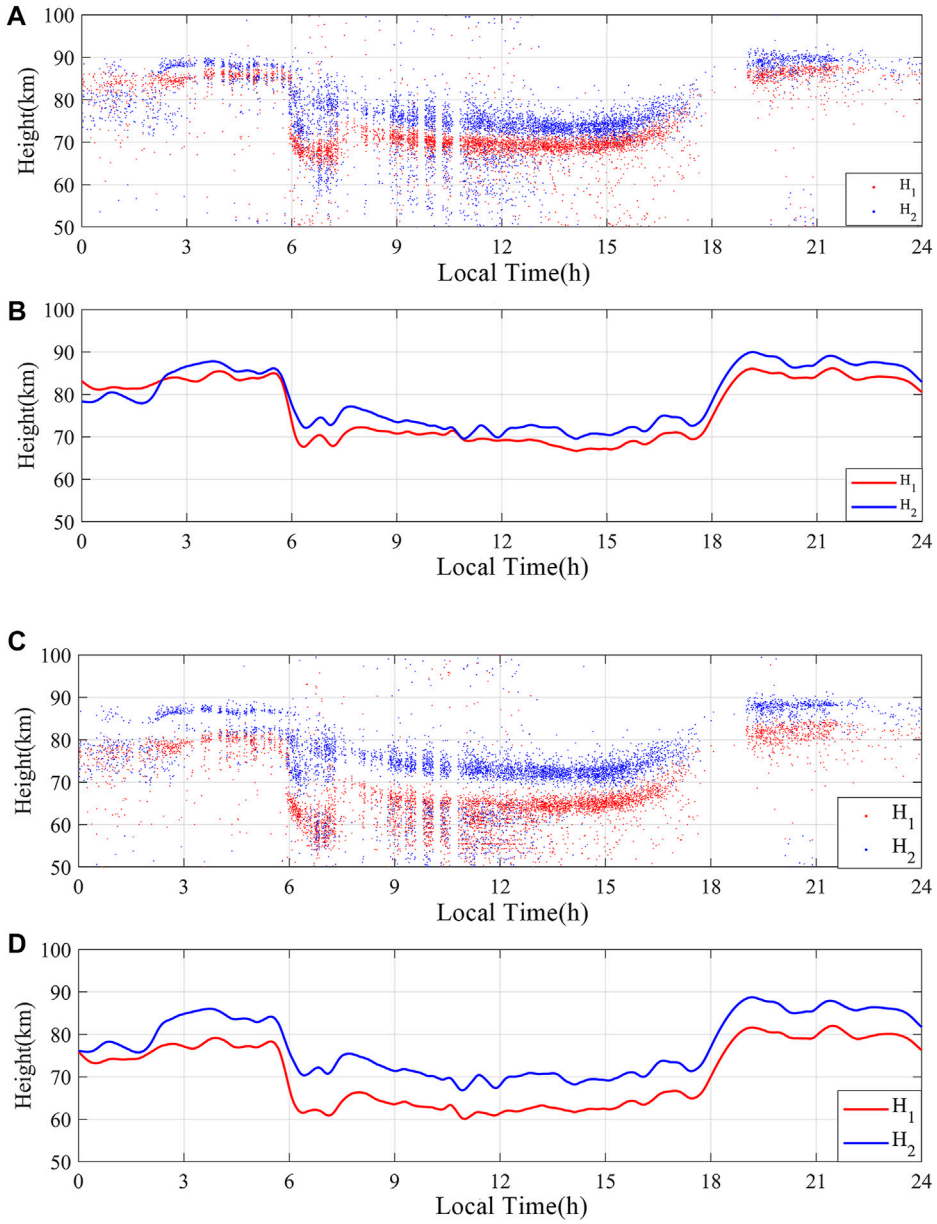

FIGURE 6
The scatter and line graphs of the ionosphere reflection heights in the ionosphere D region (Local Time: UT+8). **(A)** Scatter graph and without considering time delay; **(B)** Line graph and without considering time delay. **(C)** Scatter graph and considering time delay; **(D)** Line graph and considering time delay.

average fitted curves can be considered close to the results for the three different current sources. Thus, we used the average fitting curve to revise the ground wave arrival time delay and applied the revised ground wave arrival time in the following work.

3 Results and analysis

3.1 Temporal variations of continuous 24 h

Figures 6A, B show the scatter and line graphs of the ionosphere equivalent reflection height with time delay. From 00:00 to 05:30 LT (local time: UT + 8), H_1 fluctuated in the range of 81 km–85 km, while H_2 had a wider fluctuation range between 77 and 88 km. At 5:30 LT, the height was rapidly dropping, and the drop lasted for approximately 1 hour. Between 06:30 and 17:30 LT, the height was relatively stable. This fluctuation may be due to the low amount of data in part of the time period, which led to anomalous values that affected the fitting results. H_1 fluctuated in the range of 67.7 km–72.2 km, while H_2 fluctuated in the range of 72.1 km–77 km. The height in the daytime showed a significant increase compared to the results in Figures 6C, D, especially for H_1. At 17:30 LT, the height showed an upward trend

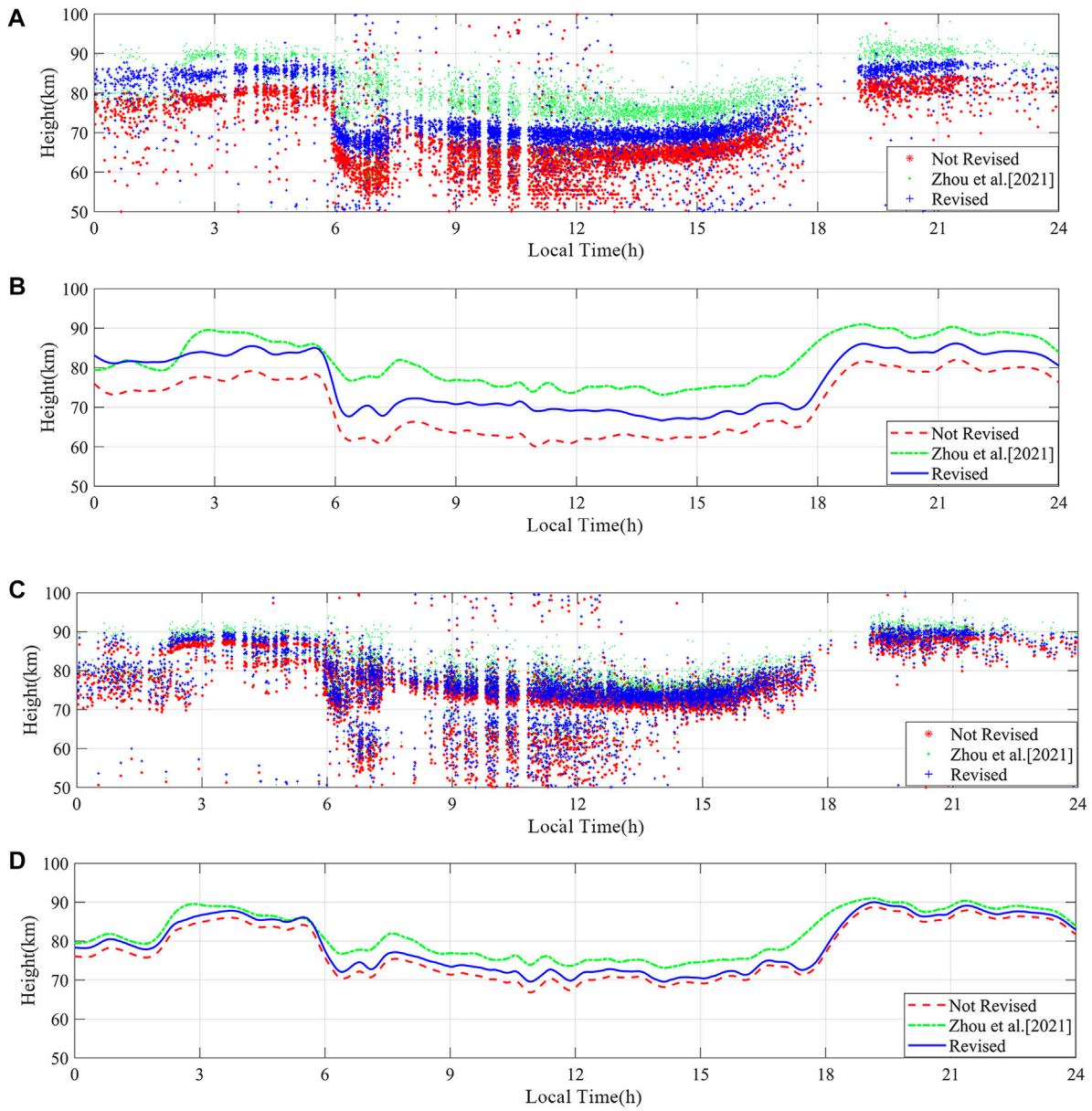

FIGURE 7
H_1 and H_2 plotted by different methods (local time: UT+8). **(A)** Scatter graph of H_1. **(B)** Line graph of H_1. **(C)** Line graph of H_2. **(D)** Line graph of H_2.

and remained relatively stable between 20:00 and 23:59 LT. H_1 fluctuated in the range of 80 km–86 km, while H_2 fluctuated in the range of 82 km–89 km.

Figures 6C, D show the scatter and line graphs of the ionosphere equivalent reflection height without considering the time delay. The trend of the height changes over time in the figure is close to the result in Figures 6A, B; however, the calculated height is slightly lower than that obtained by considering the time delay. From 00:00 to 05:30 LT, H_1 fluctuated in the range of 73 km–79 km, and H_2 fluctuated from 76 km to 86 km. During the daytime, H_1 and H_2 fluctuated from 61 km to 66.7 km and 70.8 km–75.4 km, respectively. After a rapid upward change, between 20:00 and 23:59 LT, H_1 fluctuated between 76 km and 82 km, and H_2 fluctuated between 81 km and 88 km.

Figure 6 demonstrates that when a time delay is considered, the height difference between H_1 and H_2 is significantly smaller, which is closer to the model assumptions indicated previously and verifies the method.

To further illustrate the reliability of the revised method in this study, the curve of the ionosphere equivalent reflection height variation with time was plotted using the method proposed by Zhou et al. (Azadifar et al., 2017). It should be noted that the "revised" and "not revised" in this study refer to the revision of the ground wave arrival time. It is significant to note that the approach described by Zhou presupposed that $H_1 = H_2$; hence, only one curve may be provided. As shown in Figure 7, the two methods have fairly similar results regarding the trend of fluctuations in the ionosphere equivalent reflection height.

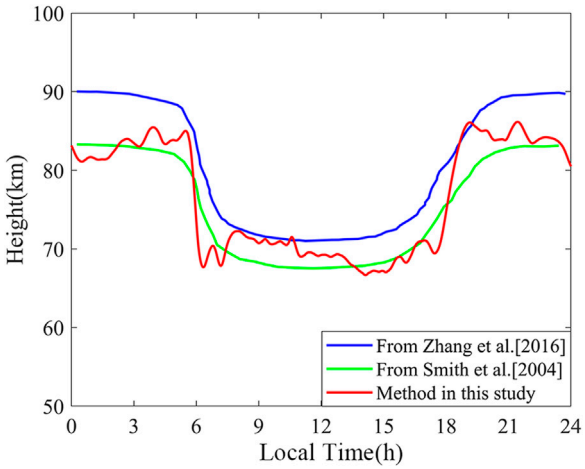

FIGURE 8
Diurnal variation in the reflection height of the ionosphere D region compared with those reported by Zhang et al. (Thomson et al., 2007) and Smith et al. (2004) (local time: UT+8).

The Consultative Committee on International Radio (CCIR) recommends an ionosphere equivalent reflection height at night and noon of about 87 km and 70 km, respectively (Azadifar et al., 2017), which is consistent with the results obtained in this study. These comparisons show that when lightning occurs over a long distance, the calculated height will be slightly lower due to the effect of delayed ground wave time. The method proposed in this study can better revise this error and increase the reliability of the height measurement value, which also supports the subsequent distance estimation using the ionosphere reflection height.

The H_1 obtained using the methodology presented in this study was roughly between 67 km and 72 km during the daytime and between 80 km and 86 km at night. H_2 was generally estimated at between 80 and 90 km at night and 70 km at noon. Han and Cummer (2010) reported an average ionosphere height of 84.9 km in the D region, ranging from 82.0 km to 87.2 km at night. The result obtained by Thomson et al. (2007), 85.1 ± 0.4 km, was consistent with the results in the present study. Figure 8 shows that the trend in ionosphere equivalent reflection over time was consistent with the curves measured by Smith et al. (2004) and Zhang et al. (2016). The difference in the figure was mainly due to differences in measurement methods and also proves that the method used in the present study is reliable at longer distances.

3.2 Distance estimation using the revised time delay

The distance between the lightning source and the single site can be obtained by using the time difference between the arrival times of the ground wave and skywaves. The arrival time difference (T_1) between the ground wave and the first skywave was selected to minimize the impact of electromagnetic waves during long-distance

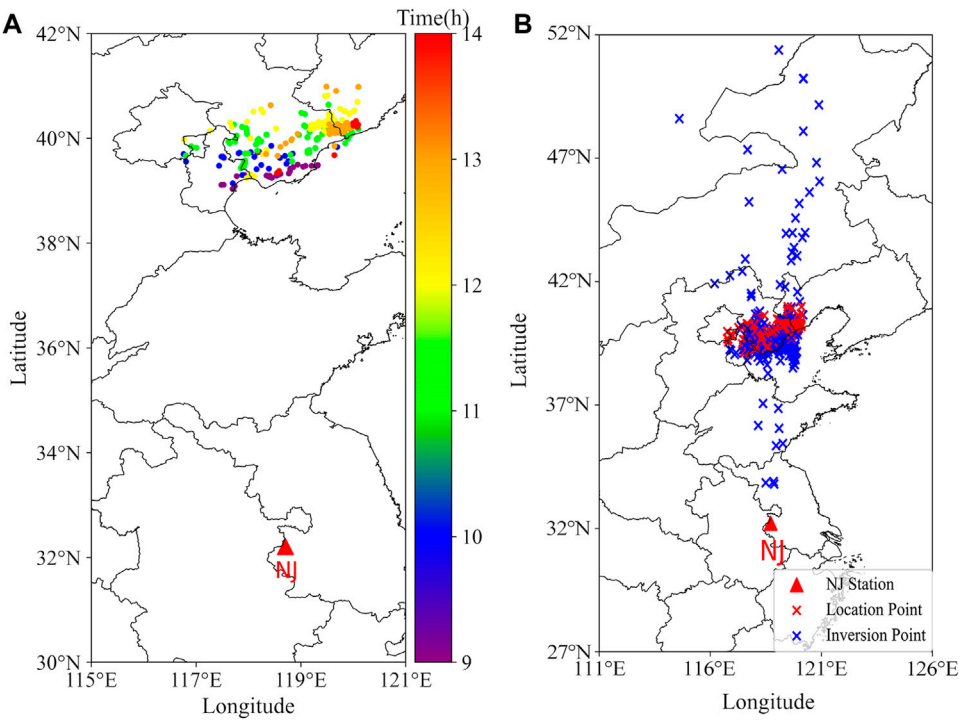

FIGURE 9
Estimated lightning distance by a single site. **(A)** Distributions of lightning events in selected regions on 3 October 2021, from 09:00 to 15:00 (local time: UT+8). **(B)** Single-site distance estimation results *versus* multi-station.

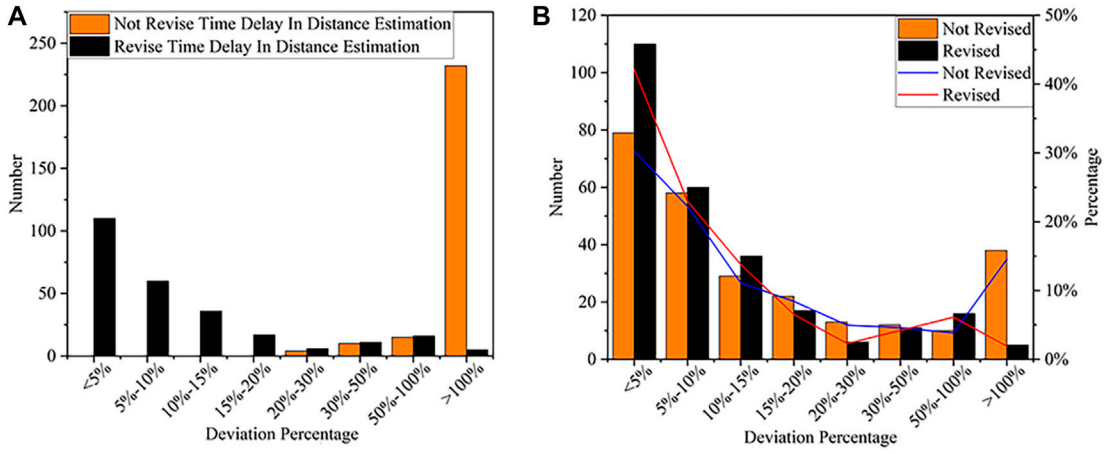

FIGURE 10
Relative deviation in single-station distance estimation. **(A)** Considering a ground wave peak time delay in distance estimation. **(B)** Comparing the revised method with the non-revised method.

propagation. H_1 and T_1 were substituted into Eq. 13 through iteration to solve the distance between the lightning and the station. As shown in Figure 9A, a daytime process in the region of 762 km–982 km from Nanjing station on 13 October 2021, was selected. The location results are shown in Figure 9B, with a total of 261 sets of data. The red crosses represent the location results for multiple stations, while the blue crosses are the results for a single site. In this study, we only compared the difference in distance. The azimuth of lightning refers to the results obtained from multiple stations. Most of the single-site results were relatively concentrated.

Figures 10, 11 show the relative and absolute deviations of the single-site distance estimation, respectively, using the multiple-station lightning location results as a reference. Figure 10A compares the difference between revising and not revising the ground wave time delay only for the distance estimation. Since the ground wave time delay was considered in calculating the ionosphere equivalent reflection height, not considering the delay in distance estimation will result in deviation from the true value. Figure 10B compares the results of the revised method proposed in this study with the method that does not consider the ground wave time delay. The distance estimation accuracy was also significantly improved. The percentage of data with errors within 10% increased from 52% to 65% and the percentage of data with errors >100% decreased from 18% to 8%.

The absolute deviation of the single-site distance estimate is given in Figure 11. The treatment in the figure refers to whether the ground wave arrival time was revised in the distance estimation, N total indicates the number of data in each data group, and the bar chart represents the average absolute deviation. For the overall results of the distance estimates for the 261 lightning events in Figure 9, when the ground wave time delay was revised in calculating the ionosphere equivalent height and estimating the lightning occurrence distance, the absolute average error was 128.22 km; however, when the ground wave time delay was revised only in estimating the lightning occurrence distance and the ionosphere equivalent reflection height was calculated without considering the ground wave time delay, the absolute average error was 246.04 km. Thus, the ground wave time delay considerably impacted the precision of the distance estimate for the single-site lightning location. The average deviation of the entire data set in Figure 11A shows that revising the ground wave time delay could effectively reduce the inaccuracy of distance estimation.

To understand whether the proposed method will have the problem of decreasing accuracy with increasing distance, the statistical results of five distance bands are given in Figure 11. The average error increased with increasing distance. However, the deviation in the distance estimation in the range of 806 km–850 km was only 48.07 km, significantly better than the results for closer distances. Therefore, the method proposed in this study still applies to lightning that occurs at long distances. Moreover, for each distance band in the optimal group, the distance deviation of our proposed revised method was generally smaller than that of the original method, except for the 938 km–982 km distance interval. However, only seven data samples occurred in this interval.

The results of the distance estimates showed some data with errors >100%. Comparison of the revised and non-revised methods revealed a certain set of data with large deviations using both methods, ruling out the possibility that the method influenced these results. Considering that these reflected data with a longer time scale, this situation may occur due to variation in the ionosphere equivalent reflection height at different times. To verify this conjecture, Figure 12 represents a scatter plot of the error distribution with time, showing that the data with errors >100% are distributed over various periods and unrelated to the ionosphere equivalent reflection height variation. Figure 12 shows more intuitively that the method proposed in this paper significantly improved the estimation accuracy.

Since the variables used to solve the distance in Eq. 13 were the arrival time difference between the skywave and the ground wave,

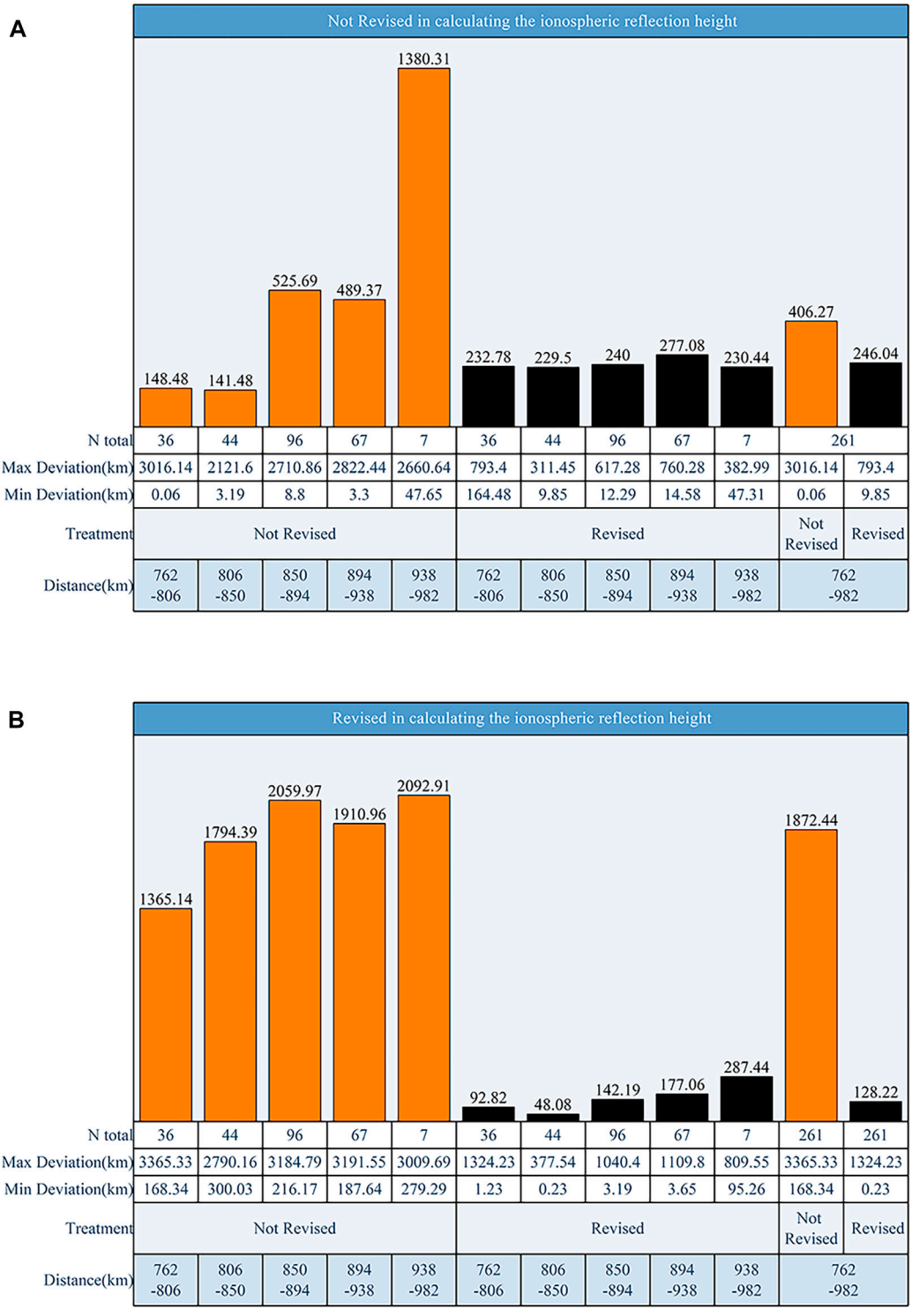

FIGURE 11
Histogram of single-station distance estimation error. Distance estimation using ionosphere heights obtained by unrevised **(A)** and **(B)** revised ground wave arrival time delays.

further inspection of the data revealed that for these data with errors >100%, the arrival time difference was much smaller than the other data. This may occur due to noise interference during the propagation process, resulting in a shift in the peak points of the ground wave or the first skywave, which, in turn, affects the accuracy of the estimation results.

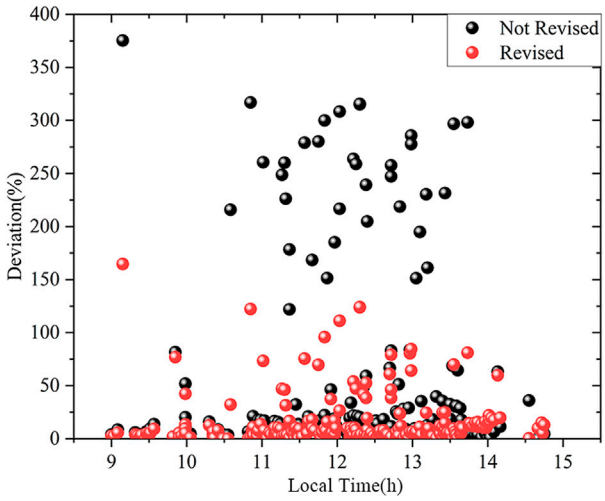

FIGURE 12
Scatter plot of error at different times (local time: UT+8).

TABLE 2 Comparison between existing methods and the current method on the single-site lightning location.

Method	Distance (km)	Error (%)
Nagano et al. (2007)	200 km	12.5%
Chen et al. (2015)	<130 km	15.5%–20%
The method in this paper	762 km–982 km	14.6%

4 Discussion

Based on the phenomenon that the ground wave arrival time will lag during long-distance propagation, we analyzed the effect of the curvature of the Earth and ground finite conductivity on the sferics waveform using the numerical method and statistically analyzed the delay in the arrival time of the far-field waveform. The delay time was also used to calculate the ionosphere equivalent reflection height and estimate the lightning distance using a single site.

The results of the estimated distances for a single site in Section 3 show an average error of 128.8 km. The comparison between the method used in this study and other methods is shown in Table 2. The data selected in the compared methods were mainly lightning data at close distances (~200 km), while lightning data used in this study occurred between 700 km and 900 km. Some places, such as islands, forests, military bases, and ocean-going vessels, lack good network transmission capability or have many limitations in transmitting to external networks. Because the transmission with external networks is limited, it is impossible to establish a multi-station lightning location system and obtain the lightning location results given by other lightning location networks or the acquisition cost is relatively higher. The single-site lightning location system does not need to rely on high-precision time modules and the Internet to provide real-time lightning location results, and the operating cost is low. Due to the propagation effect, the arrival time difference between the first skywave and the ground wave in the actual waveform is much smaller than the ideal condition as the propagation distance of LEMP increases, which leads to an increasing deviation of the distance estimation results as the propagation distance increases. Therefore, the method proposed in this work may be an excellent solution to this problem. In this study, the relationship between the ground wave arrival time delay and the propagation distance obtained by the numerical algorithm could well correct the ground wave arrival time delay. The average error in Figure 11 shows that the average absolute deviation of distance estimation was reduced by 117.85 km when the ground wave arrival time delay was revised, thus demonstrating that the reliability of long-range lightning detected by the single site can be improved using the method proposed in this study. Moreover, the single-site lightning detection system proposed in this study can reach a detection range of 900 km. More reliable location results for long-range lightning can allow lightning risk warnings, prediction of lightning activity trends, and other functions, which have engineering applications.

Analysis of the waveform data showed that the data with large deviation values were mainly because of effects on the sferics by noise during propagation, resulting in different degrees of distortion in the received waveform. Thus, when matching with the waveform bank, the actual waveform is matched to the simulation waveform at a longer distance, resulting in deviations in the actual sferics peak points obtained according to the matching. The time difference between the skywave and ground wave peak points decreases, while the deviation of the estimated distance result increases.

The error in the distance estimation in this study mainly came from two aspects:

(1) The waveform bank used for waveform matching was simulated by two-dimensional FDTD without fully considering the influence of the geomagnetic field, which differs from the actual lightning waveform, especially in the skywave.
(2) In the calculation of the ground wave time delay, we assumed that the ground conductivity was 0.01 S/m and the ground was smooth. However, in the actual propagation process, we also need to consider the influence of the terrain on the lightning waveform.

5 Conclusion

In this study, the time delay *versus* distance curve was obtained by a numerical algorithm, which considered the ground wave time delay in the long-distance propagation process caused by the curvature of the Earth and the finite conductivity of the ground. This error was corrected by calculating the ionosphere equivalent reflection height to improve the reliability of the results. The accuracy of single-site estimation was evaluated using multi-station data. The main conclusions of this paper are as follows:

(1) In this work, we fit the time arrival delay *versus* the distance curve for the ground wave peak using a numerical algorithm.

The ground wave time arrival delay *versus* distance showed a roughly linear relationship, with an average arrival time delay of 0.9 μs (compared with the arrival time at the speed of light) for every 100 km increase in propagation distance.

(2) The time difference between the actual sferics ground wave and the skywave peaks was identified by waveform bank matching and peak identification. The time delay was revised to calculate the ionosphere equivalent reflection height. For H_1 and H_2, the height ranges were 80 km–86 km and 77 km–89 km at night and 66 km–72 km and 69 km–77 km at daytime, respectively. Compared with the results without the time delay, the overall curves were higher by an average of 6 km–9 km.

(3) For a total of 261 lightning events occurring at the distance of 700 km–900 km from the single site, the distance estimation results obtained by the single-site system were compared with those of the multi-station lightning location and showed an average error of 128.8 km (14.6%) and a median distance error of 52.6 km. The average error of the results without considering the time delay was 246.04 km (45.9%). The percentage of distance estimation results with relative errors within 10% increased from 52% to 65%.

It should be noted that the proposed method is also applicable to lightning events at longer distances if sufficient data are available. In future research, we will combine the magnetic direction finder (MDF) to implement lightning location estimation and verify the accuracy of the method for estimating lightning at longer distances. We will also collect more data to build a bank of real waveforms by machine learning to improve the accuracy of waveform peak matching and further investigate the effects of different propagation directions and different terrain on the ionosphere equivalent reflection height.

Data availability statement

The original contributions presented in the study are included in the article/supplementary material. further inquiries can be directed to the corresponding author.

Author contributions

Conceptualization, JiZ and QZ; Data curation, JiZ, JuZ, BD, YW, JZe and LS; Formal analysis, JiZ, JL, JY and JG; Funding acquisition, QZ; investigation, JiZ and QZ; methodology, JiZ and JuZ; software, JiZ; JuZ and JL; supervision, QZ; visualization, JiZ; writing—original draft, JiZ; writing—review and editing, QZ. All authors contributed to the article and approved the submitted version.

Funding

This research was funded by the National Natural Science Foundation of China (grant 41775006).

Acknowledgments

The authors thank the National Satellite Meteorological Center (NSMC) of the China Meteorological Administration for providing the FY4A-AGRI dataset. The author would like to thank the people and departments involved in the construction of the network. The authors would also like to thank the reviewers for their helpful feedback, which significantly improved the manuscript.

Conflict of interest

The authors declare that the research was conducted in the absence of any commercial or financial relationships that could be construed as a potential conflict of interest.

Publisher's note

All claims expressed in this article are solely those of the authors and do not necessarily represent those of their affiliated organizations, or those of the publisher, the editors, and the reviewers. Any product that may be evaluated in this article, or claim that may be made by its manufacturer, is not guaranteed or endorsed by the publisher.

References

Ammar, A., and Ghalila, H. (2020). Estimation of nighttime ionospheric D-region parameters using tweek atmospherics observed for the first time in the North African region. *Adv. Space Res.* 66 (11), 2528–2536. doi:10.1016/j.asr.2020.08.025

Azadifar, M., Li, D., Rachidi, F., Rubinstein, M., Diendorfer, G., Schulz, W., et al. (2017). Analysis of lightning-ionosphere interaction using simultaneous records of source current and 380 Km distant electric field. *J. Atmos. Solar-Terrestrial Phys.* 159, 48–56. doi:10.1016/j.jastp.2017.05.010

Carvalho, F. L., Uman, M. A., Jordan, D. M., Hill, J. D., Cummer, S. A., Kotovsky, D. A., et al. (2017). Triggered lightning sky waves, return stroke modeling, and ionosphere effective height: Triggered lightning sky waves. *J. Geophys. Res. Atmos.* 122 (6), 3507–3527. doi:10.1002/2016JD026202

Chen, M., Lu, T., and Du, Y. (2015). An improved wave impedance approach for locating close lightning stroke from single station observation and its validation. *J. Atmos. Solar-Terrestrial Phys.* 122, 1–8. doi:10.1016/j.jastp.2014.11.001

Cummer, S. A., Inan, U. S., and Bell, T. F. (1998). Ionospheric*D*region remote sensing using VLF radio atmospherics. *Radio Sci.* 33 (6), 1781–1792. doi:10.1029/98RS02381

Dennis, A. S., and Pierce, E. T. (1964). The return stroke of the lightning flash to Earth as a source of VLF atmospherics. *Radio Sci.* 68D, 777. doi:10.6028/jres.068d.075

Han, F., and Cummer, S. A. (2010). Midlatitude nighttime D region ionosphere variability on hourly to monthly time scales: D region measurement. *J. Geophys. Res.* 115 (A9), n/a–n. doi:10.1029/2010ja015437

Heidler, F., Cvetic, J. M., and Stanic, B. V. (1999). Calculation of lightning current parameters. *IEEE Trans. Power Deliv.* 14 (2), 399–404. doi:10.1109/61.754080

Hill, D. A., and Wait, J. R. (1980). Ground wave attenuation function for a spherical earth with arbitrary surface impedance. *Radio Sci.* 15, 637–643. doi:10.1029/RS015i003p00637

Honma, N., Suzuki, F., Miyake, Y., Ishii, M., and Hidayat, S. (1998). Propagation effect on field waveforms in relation to time-of-arrival technique in lightning location. *J. Geophys. Res.* 103 (D12), 14141–14145. doi:10.1029/97JD02625

Hou, W., Azadifar, M., Rubinstein, M., Rachidi, F., and Zhang, Q. (2020). The polarity reversal of lightning-generated sky wave. *J. Geophys. Res. Atmos.* 125, e2020JD032448. doi:10.1029/2020jd032448

Hou, W., Zhang, Q., Zhang, J., Wang, L., and Shen, Y. (2018). A new approximate method for lightning-radiated ELF/VLF ground wave propagation over intermediate ranges. *Int. J. Antennas Propag.* 2018, 1–10. doi:10.1155/2018/9353294

Hu, W., and Cummer, S. A. (2006). An FDTD model for low and high altitude lightning-generated EM fields. *IEEE Trans. Antennas Propagat.* 54 (5), 1513–1522. doi:10.1109/TAP.2006.874336

Inan, U. S., Cummer, S. A., and Marshall, R. A. (2010). A survey of ELF and VLF research on lightning-ionosphere interactions and causative discharges: Elf and VLF signatures of lightning. *J. Geophys. Res.* 115 (6), n/a. doi:10.1029/2009ja014775

Jacobson, A. R., Holzworth, R., and Shao, X.-M. (2008). Low-frequency ionospheric sounding with narrow bipolar event lightning radio emissions: Energy-reflectivity spectrum. *Ann. Geophys.* 26 (7), 1793–1803. doi:10.5194/angeo-26-1793-2008

Koochak, Z., and Fraser-Smith, A. (2020). Single-station lightning location using azimuth and time of arrival of sferics. *Radio Sci.* 55 (2). doi:10.1029/2018RS006627

Lay, E. H., and Shao, X.-M. (2011). High temporal and spatial-resolution detection of D-layer fluctuations by using time-domain lightning waveforms: Detection of d-layer fluctuations. *J. Geophys. Res.* 116 (A1), n/a. doi:10.1029/2010ja016018

Lay, E. H., and Shao, X.-M. (2011). Multi-station probing of thunderstorm-generated D-layer fluctuations by using time-domain lightning waveforms: MULTI-STATION VLF measurement of d-layer. *Geophys. Res. Lett.* 38 (23), n/a. doi:10.1029/2011GL049790

Li, J., Dai, B., Zhou, J., Zhang, J., Zhang, Q., Yang, J., et al. (2022). Preliminary application of long-range lightning location network with equivalent propagation velocity in China. *Remote Sens.* 14 (3), 560. doi:10.3390/rs14030560

Mostajabi, A., Karami, H., Azadifar, M., Ghasemi, A., Rubinstein, M., and Rachidi, F. (2019). Single-sensor source localization using electromagnetic time reversal and deep transfer learning: Application to lightning. *Sci. Rep.* 9 (1), 17372. doi:10.1038/s41598-019-53934-4

Nagano, I., Yagitani, S., Ozaki, M., Nakamura, Y., and Miyamura, K. (2007). Estimation of lightning location from single station observations of sferics. *Electron. Comm. Jpn. pt. I* 90 (1), 25–34. doi:10.1002/ecja.20329

Nucci, C. A., Mazzetti, C., Rachidi, F., and Ianoz, M. (1988). *On lightning return stroke models for LEMP calculations, paper presented at 19th International Conference on Lightning Protection*. Graz, Austria: Assoc.

Ogawa, T., and Komatsu, M. (2007). Analysis of Q Burst waveforms: Analysis of Q burst waveforms. *Radio Sci.* 42 (2), n/a. doi:10.1029/2006rs003493

Rachidi, F., Janischewskyj, W., Hussein, A. M., Nucci, C., Guerrieri, S., Kordi, B., et al. (2001). Current and electromagnetic field associated with lightning-return strokes to tall towers. *IEEE Trans. Electromagn. Compat.* 43 (3), 356–367. doi:10.1109/15.942607

Ramachandran, V., Prakash, J. N., Deo, A., and Kumar, S. (2007). Lightning stroke distance estimation from single station observation and validation with WWLLN data. *Ann. Geophys.* 25 (7), 1509–1517. doi:10.5194/angeo-25-1509-2007

Shao, X.-M., and Jacobson, A. R. (2009). Model simulation of very low-frequency and low-frequency lightning signal propagation over intermediate ranges. *IEEE Trans. Electromagn. Compat.* 51 (3), 519–525. doi:10.1109/TEMC.2009.2022171

Shao, X.-M., Lay, E. H., and Jacobson, A. R. (2013). Reduction of electron density in the night-time lower ionosphere in response to a thunderstorm. *Nat. Geosci.* 6 (1), 29–33. doi:10.1038/ngeo1668

Smith, D. A., Heavner, M. J., Jacobson, A. R., Shao, X. M., Massey, R. S., Sheldon, R. J., et al. (2004). A method for determining intracloud lightning and ionosphere heights from VLF/LF electric field records: VLF/LF IC lightning and ionosphere height. *Radio Sci.* 39 (1), n/a. doi:10.1029/2002rs002790

Somu, V. B., Rakov, V. A., Haddad, M. A., and Cummer, S. A. (2015). A study of changes in apparent ionospheric reflection height within individual lightning flashes. *J. Atmos. Solar-Terrestrial Phys.* 136, 66–79. doi:10.1016/j.jastp.2015.09.007

Thomson, N. R., Clilverd, M. A., and McRae, W. M. (2007). Nighttime ionosphere D region parameters from VLF phase and amplitude: Night ionosphere D region parameters. *J. Geophys. Res.* 112 (7), n/a. doi:10.1029/2007ja012271

Tran, T. H., Baba, Y., Somu, V. B., and Rakov, V. A. (2017). FDTD modeling of LEMP propagation in the Earth-ionosphere waveguide with emphasis on realistic representation of lightning source. *J. Geophys. Res. Atmos.* 122 (12), 937. doi:10.1002/2017sJD027305

Wait, J. R. (1974). Recent analytical investigations of electromagnetic ground wave propagation over inhomogeneous earth models. *Proc. IEEE* 62, 1061–1072. doi:10.1109/PROC.1974.9570

Wang, J., Xiao, F., Yuan, S., Song, J., Ma, Q., and Zhou, X. (2022). A novel method for ground-based VLF/LF single-site lightning location. *Measurement* 196, 111208. doi:10.1016/j.measurement.2022.111208

Zhang, H., Lu, G., Qie, X., Jiang, R., Fan, Y., Tian, Y., et al. (2016). Locating narrow bipolar events with single-station measurement of low-frequency magnetic fields. *J. Atmos. Solar-Terrestrial Phys.* 143–144, 88–101. doi:10.1016/j.jastp.2016.03.009

Zhang, J., Zhou, J., Li, J., Gu, J., Zhang, Q., Dai, B., et al. (2022). Location accuracy improvement of long-range lightning detection network in China by compensating ground wave propagation delay. *Remote Sens.* 14, 3397. doi:10.3390/rs14143397

Zhou, X., Wang, J., Ma, Q., Huang, Q., and Xiao, F. (2021). A method for determining D region ionosphere reflection height from lightning skywaves. *J. Atmos. Solar-Terrestrial Phys.* 221, 105692. doi:10.1016/j.jastp.2021.105692